CONFERENCE PRE-PRINT

NONLINEAR MAGNETOHYDRODYNAMIC MODELLING OF IDEAL BALLOONING MODES IN HIGH- β WENDELSTEIN 7-X PLASMAS

YAO ZHOU Shanghai Jiao Tong University Shanghai, China Email: yao.zhou@sjtu.edu.cn

K. ALEYNIKOVA Max-Planck-Institut für Plasmaphysik Greifswald, Germany

CHANG LIU Peking University Beijing, China

N.M. FERRARO Princeton Plasma Physics Laboratory Princeton, NJ, United States

Abstract

This paper presents nonlinear magnetohydrodynamic (MHD) simulations of high- β W7-X plasmas using the stellarator extension of M3D- C^1 , building on the recent work that shows benign saturation of ideal ballooning modes above the designed β limit in the standard configuration. First, the sensitivity to the parallel thermal conductivity is examined. It is found that while an increased parallel conductivity reduces the linear growth rate, the saturated pressure profile is barely affected. Second, the dependence on the shape of the pressure profile is considered. It is shown that an equilibrium with a peaked profile and lower β is subject to more significant change than a broad profile and higher β , suggesting that benign saturation, or nonlinear stability, is not guaranteed. Third, the impact of the magnetic configuration is studied, with the equilibrium rotational transform varied by adjusting the planar coil current. It is found that similar growth rates result in similar magnitudes of profile change regardless of the presence of a low-order resonance, which implies that the core activities that lead to the degradation may be of non-resonant nature. These results indicate that MHD stability should still be treated seriously in stellarator operation and design, for which nonlinear modelling using tools like M3D- C^1 can play an instrumental role.

1. INTRODUCTION

The stellarator is one of the most promising concepts for future fusion reactors, featuring unique advantages in steady-state operation by avoiding challenges associated with the maintenance and stability of the plasma current [1]. The experimental findings of the advanced Wendelstein 7-X (W7-X) stellarator have successfully demonstrated that optimized magnetic configurations can significantly improve plasma confinement, achieving record-breaking stellarator fusion-triple-product values with modest heating power [2]. Henceforth, W7-X has been equipped with water-cooled divertors and enhanced fueling and heating capabilities that enabled further progress in extended high-performance operation [3, 4]. Ultimately, the continuous, reactor-relevant operation of W7-X will have profound implications on the viability of the stellarator concept, and its success critically depends on maintaining magnetohydrodynamic (MHD) stability at high β (which denotes the volume-averaged ratio of plasma to magnetic pressure throughout this paper).

The designed β -limit of W7-X is about 5% based on linear MHD stability analysis [5, 6], but stellarator plasmas have shown nonlinear stability when driven beyond linear stability thresholds in experiments [7]. Recently, we reported the first nonlinear MHD simulations of pressure-driven instabilities in high- β W7-X plasmas [8], which were enabled by the stellarator extension of the M3D- C^1 code [9]. In the standard configuration, the simulation

results agree with the design analysis that ideal ballooning modes become linearly unstable when β exceeds 5%, but predict nonlinear saturation at benign levels with mild confinement degradation, which is much less severe than the original expectation of losing the plasma column. This suggests that W7-X may be able to operate at or slightly above the designed β -limit while avoiding major MHD events, and enhances the appeal of the stellarator approach to steady-state fusion reactors. However, the conclusion needs to be further examined since the results can be sensitive to simulation parameters, profile shapes, magnetic configurations, etc.

In this paper, we build on Ref. [8] and present more comprehensive MHD simulations of ideal ballooning modes in high- β W7-X plasmas. First, we examine the sensitivity to the parallel thermal conductivity. It is found that while an increased parallel conductivity reduces the linear growth rate, the saturated change of the pressure profile is barely affected. Second, we consider the dependence on the shape of the pressure profile. It is shown that an equilibrium with a peaked profile and lower β is subject to more significant change than a broad profile and higher β , suggesting that benign saturation, or nonlinear stability, is not guaranteed. Third, we study the impact of the magnetic configuration, varying the equilibrium rotational transform by adjusting the planar coil current. It is found that similar growth rates result in similar magnitudes of profile change regardless of the presence of a low-order resonance, which implies that the core activities that lead to the degradation may be of non-resonant nature. These results indicate that MHD stability should still be treated seriously in stellarator operation and design, for which nonlinear modelling using tools like M3D- C^1 can play an instrumental role.

This paper is organized as follows. In Section 2 we introduce the M3D-C1 code and the simulation settings. In Section 3 we analyze the sensitivity of linear growth and nonlinear saturation with respect to the parallel heat conductivity. In Section 4 we show that a peaked pressure profile is subject to more pronounced ballooning-induced degradation than a broad profile. In Section 5 we study how the saturated state depends on the equilibrium iota. Summary and discussion follow in Section 6.

2. SIMULATION SETTINGS

M3D- C^1 is a sophisticated nonlinear MHD code designed to model the macroscopic dynamics of toroidal fusion plasmas [10]. For temporal discretization, M3D- C^1 implements a split-implicit scheme that realizes stable and efficient transport-timescale simulations [11]. For spatial discretization, M3D- C^1 employs high-order finite elements with C^1 continuity in three dimensions and has been successfully extended to stellarator geometry [9]. Recent simulations of current-drive-induced sawtooth-like crashes in W7-X validates this new capability by showing semi-quantitative agreements with experimental results [12]. While two-fluid and many other effects are available in M3D- C^1 , their functionality has not yet been fully verified in stellarator geometry. So in this work, we solve the single-fluid extended MHD equations (in SI units)

$$\partial_t \rho + \nabla \cdot (\rho \mathbf{v}) = D \nabla^2 (\rho - \rho_0), \tag{1}$$

$$\rho(\partial_t \mathbf{v} + \mathbf{v} \cdot \nabla \mathbf{v}) = \mathbf{j} \times \mathbf{B} - \nabla p - \nabla \cdot \mathbf{\Pi},\tag{2}$$

$$\partial_t p + \mathbf{v} \cdot \nabla p + \gamma p \nabla \cdot \mathbf{v} = (\gamma - 1)[\eta(j^2 - j_0^2) - \nabla \cdot \mathbf{q} - \mathbf{\Pi} : \nabla \mathbf{v}], \tag{3}$$

$$\partial_t \mathbf{B} = \nabla \times [\mathbf{v} \times \mathbf{B} - \eta(\mathbf{j} - \mathbf{j}_0)], \tag{4}$$

for the mass density ρ , velocity \mathbf{v} , pressure p, and magnetic field \mathbf{B} , with the current density $\mathbf{j} = \mu_0^{-1} \nabla \times \mathbf{B}$ and the adiabatic index $\gamma = 5/3$. The viscous stress tensor is $\mathbf{\Pi} = -\mu(\nabla \mathbf{v} + \nabla \mathbf{v}^T) - 2(\mu_c - \mu)(\nabla \cdot \mathbf{v})\mathbf{I}$ and the heat flux $\mathbf{q} = -\kappa_{\perp} \nabla (T - T_0) - \kappa_{\parallel} \mathbf{b} \mathbf{b} \cdot \nabla T$ with $\mathbf{b} = \mathbf{B}/B$ and the temperature $T = Mp/\rho$, where M is the ion mass.

The transport coefficients used include uniform mass diffusivity $D=2.18~\mathrm{m}^2/\mathrm{s}$, isotropic and compressible viscosities $\mu=\mu_\mathrm{c}=3.65\times10^{-7}~\mathrm{kg/(m\cdot s)}$. The ratio between the parallel and perpendicular thermal conductivities, $\kappa_\parallel/\kappa_\perp$, is varied with $\kappa_\perp=2.18\times10^{20}~(\mathrm{m\cdot s})^{-1}$ (c.f. Section 3). The temperature-dependent resistivity η is enhanced by 100 times from the Spitzer resistivity and its typical value is about $10^{-6}~\Omega\cdot\mathrm{m}$ (core) to $10^{-5}~\Omega\cdot\mathrm{m}$ (edge). The equilibrium fields ρ_0 , T_0 , and \mathbf{j}_0 subtracted in the dissipative terms act as effective sources to sustain the equilibrium in the absence of instabilities. The equilibrium density and temperature profiles are $\rho_0 \propto p_0^{1/\gamma}$ and $T_0 \propto p_0^{1-1/\gamma}$. We use 3807 reduced quintic elements in the (R,Z) plane and 160 Hermite cubic elements in the toroidal direction (for a full torus). Unless otherwise noted, we use a time step size of 0.573 μ s to simulate a hydrogen plasma with a core number density of $1.5\times10^{20}~\mathrm{m}^{-3}$, such that the core temperature is about 5 keV (assuming equipartition). These settings are mostly the same as those in Ref. [8] except for the varying $\kappa_\parallel/\kappa_\perp$.

We initialize fixed-boundary stellarator simulations in M3D- C^1 using the outputs of the widely used 3D equilibrium code VMEC [13], including the geometry of the flux surfaces as well as the magnetic field \mathbf{B}_0 and the pressure p_0 . The former is given in terms of a coordinate mapping, $R(s,\theta,\varphi)$ and $Z(s,\theta,\varphi)$ with s being the normalized toroidal flux and θ the poloidal angle in VMEC, which is utilized to set up the non-axisymmetric computational domain enclosed by the last closed flux surface. (This mapping does not evolve in M3D- C^1 so that s and θ are fixed regardless of the actual dynamics of the flux surfaces.) The latter then provide the initial conditions and subtracted equilibrium fields in the simulations. The boundary conditions are ideal on the magnetic field, no-slip on the velocity, and fixed on the density and pressure.

3. SENSITIVITY TO PARALLEL THERMAL CONDUCTIVITY

In magnetically confined plasmas, heat transport is strongly anisotropic. The ratio between parallel and perpendicular thermal conductivities, $\kappa_{\parallel}/\kappa_{\perp}$, can be as high as $\sim 10^8$ according to experimental measurements [14], posing significant challenges for accurate numerical modelling. Explicit codes often adopt substantially reduced κ_{\parallel} to avoid the formidably small time steps required by numerical stability. For implicit codes, resolving realistically strong anisotropy also requires carefully designed numerical methods [11]. The high-order finite element method adopted by M3D- C^1 has been demonstrated to be effective in this aspect [15], and this favorable feature is inherited by the stellarator extension by utilizing the geometry of the flux surfaces to set up the mapping from the logical to the physical coordinates [9].

However, in practice, the ratio $\kappa_{\parallel}/\kappa_{\perp}$ is often chosen somewhat arbitrarily for convenience. For example, in Ref. [8] $\kappa_{\parallel}/\kappa_{\perp}$ is set to 10^6 and not varied. Considering that pressure dynamics can be crucial for ballooning modes, here we examine the sensitivity of their growth and saturation with respect to $\kappa_{\parallel}/\kappa_{\perp}$ using single-field-period simulations, which model 1/5 of the torus using 32 elements in the toroidal direction. Here, we consider the standard 'EIM' configuration of W7-X, specifically the $\beta=5.44\%$ equilibrium with a broad, parabolic-like pressure profile and zero current profile, and $B\approx 2.3$ T in the core. The dependence of the linear growth rate γ versus $\kappa_{\parallel}/\kappa_{\perp}$ is shown by the green curve in Fig. 1(a). It can be seen that when $\kappa_{\parallel}/\kappa_{\perp} > 10^4$, γ decreases as $\kappa_{\parallel}/\kappa_{\perp}$ increases. This demonstrates that a sufficiently large, or close-to-realistic parallel heat conductivity can suppress the linear growth of the ballooning mode.

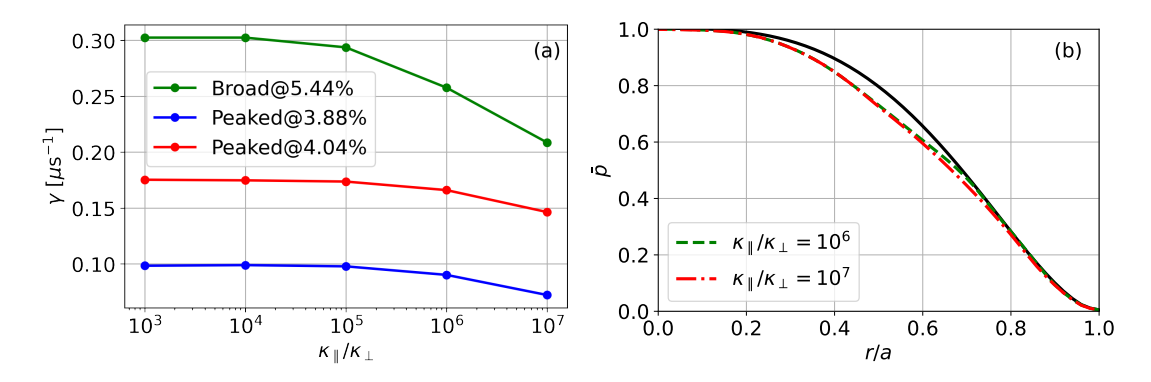


FIG. 1. (a) The linear growth rate γ vs. $\kappa_{\parallel}/\kappa_{\perp}$ in single-field-period simulations of the standard EIM configuration using a broad pressure profile (green) and a peaked pressure profile (blue and red). (b) Saturated shapes of the pressure profile in full-torus simulations using $\kappa_{\parallel}/\kappa_{\perp}=10^6$ (green dashed) and 10^7 (red dash-dot), compared with the initial broad shape (black solid). Here the normalized minor radius $r/a=\sqrt{s}$.

That said, we are mainly concerned about the nonlinear dynamics of the ballooning mode, in particular the profile change induced in full-torus simulations. In Fig. 1(b) the green dashed curve shows the saturated pressure profile obtained with $\kappa_{\parallel}/\kappa_{\perp}=10^6$ in Ref. [8], which agrees well with the red dash-dot curve obtained with $\kappa_{\parallel}/\kappa_{\perp}=10^7$. That is, despite that the linear growth rate of the ballooning mode depends on κ_{\parallel} , the final saturated state is rather insensitive. Therefore, the specific choice of $\kappa_{\parallel}/\kappa_{\perp}$ used in Ref. [8] does not have a significant impact on its main conclusion, that the ballooning modes saturate at benign levels in the standard configuration. In the following, unless otherwise noted, we use $\kappa_{\parallel}/\kappa_{\perp}=10^7$ in the simulations.

4. DEPENDENCE ON THE SHAPE OF THE PRESSURE PROFILE

So far, we have only considered the broad, parabolic-like pressure profile shown by the black curve in Fig. 1(b), where \bar{p} is the pressure normalized by its initial core value. Such a profile is favorable for achieving high volume-averaged β , and the original W7-X optimization [5, 6] presumably used similar profiles to obtain a β -limit of $\sim 5\%$ imposed by ideal ballooning instability. However, such a profile can be difficult to achieve in experiments. In fact, the pressure profiles achieved in W7-X experiments with relatively high performance tend to be more peaked [3, 4]. Therefore, in this section, we consider a more peaked profile with $\bar{p} = (1-s)^2$ as shown by the red solid curve in Fig. 2(b), and investigate how the results are affected.

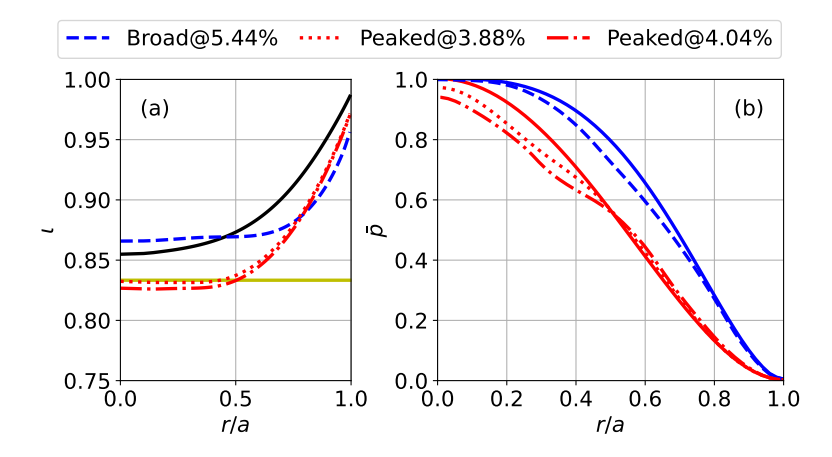


FIG. 2. (a) The rotational transform profiles in the simulated EIM equilibria, with the vacuum profile (black solid) shown for comparison. The yellow line marks the $\iota = 5/6$ resonance. (b) The final shapes of the pressure profile \bar{p} at $\theta = 0$ and $\varphi = \pi$ in the M3D-C¹ simulations, with the initial shapes (solid) shown for comparison.

Here we still consider the standard EIM configuration, specifically two equilibria with $\beta=3.88\%$ and 4.04%, respectively. Their initial rotational transform profiles are shown by the red curves in Fig. 2(a), and a notable difference from the broad-profile equilibrium (blue dashed) is the presence of $\iota=5/6$ resonances. These equilibria are found to be ideal ballooning unstable by the COBRA code [16]. For completeness, we show their linear growth rates in single-field-period M3D- C^1 simulations in Fig. 1(a), which are lower than the broad-profile case discussed in Section 3. Nevertheless, the corresponding saturated shapes of the pressure profile in Fig. 2(b) show that the peaked profile is subject to more pronounced ballooning induced degradation even with lower β and growth rates. In addition, the profile change worsens significantly as β increases slightly from 3.88% and 4.04%, while in Ref. [8] the worsening is more modest as β increases from 4.9% to 5.4%. This suggests that with a peaked pressure profile in the standard W7-X configuration, the β -limit is not only lower but also more rigid.

In Fig. 3, we compare snapshots of the pressure change δp from simulations using the broad [(a) and (b)] and peaked [(c) and (d)] profiles. Fig. 3(a) and Fig. 3(c) show coherent ballooning mode structures at the end of the linear growth, which are localized in the bad-curvature regions and radially coincide with the largest pressure gradient. That is, the modes are located near the periphery and at mid-radius for the broad and peaked profiles, respectively. The saturated pressure changes in Fig. 3(b) and Fig. 3(d) are located more radially inward compared to the linear mode structures. In particular, the degradation to the peaked profile is concentrated in the core, where an m=6 structure is clearly visible, which one naturally associates with the $\iota=5/6$ resonance shown in Fig. 2(a). This is notable since in Ref. [8], one observation of the benign saturation is the absence of strong low-n activities, which one may owe to the absence of low-n resonances in the equilibrium rotational transform. In the next section, we shall vary the magnetic configuration to see how the presence or absence of the $\iota=5/6$ resonance affects the nonlinear saturation of the ballooning modes.

5. IMPACT OF THE EQUILIBRIUM ROTATIONAL TRANSFORM

The W7-X coil system is designed with the flexibility to support a variety of magnetic configurations [17]. The standard EIM configuration is achieved when all five kinds of modular coils carry the same current, $I_{\rm MC}$. Then, the rotational transform can be adjusted by applying equal currents in the two kinds of planar coils, $I_{\rm PC}$. In this section, we adjust the ratio $I_{\rm PC}/I_{\rm MC}$ while keeping the core magnetic field and plasma volume roughly constant to generate a series of vacuum configurations, whose rotational transform profiles are shown by the black curves in

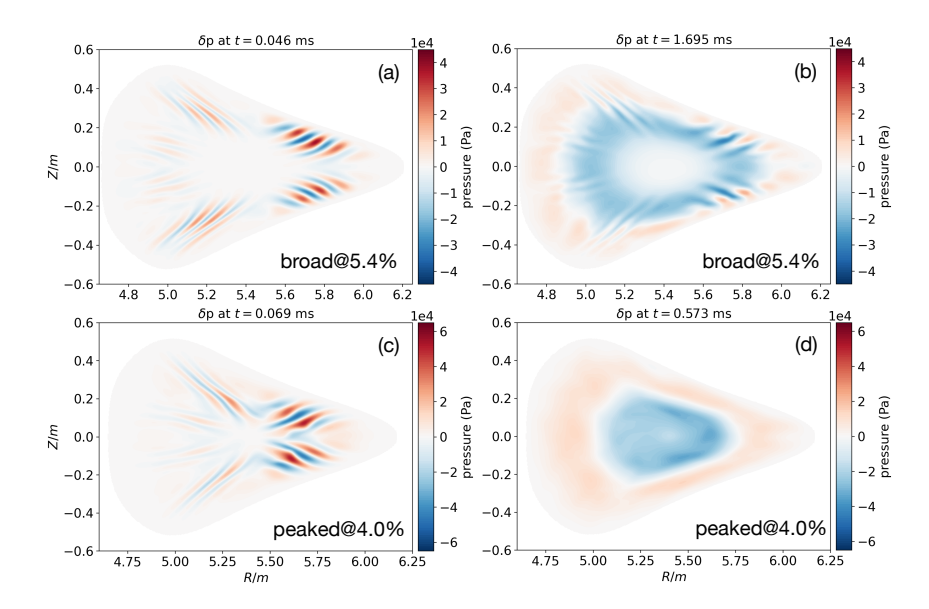


FIG. 3. Snapshots of the pressure change in two EIM simulations with different pressure profiles and beta values: (a) and (c) show mode structures at the end of the linear growth phase, while (b) and (d) show saturated states at the end of the simulations. Note the different scales in the color bars.

Fig. 4 (a) and distinguished by line styles. The solid curve is the EIM configuration in Fig. 2, and it can be seen that a positive or negative I_{PC} decreases or increases the rotational transform, respectively. Meanwhile, the shape of the profile and the magnetic shear in particular is roughly maintained.

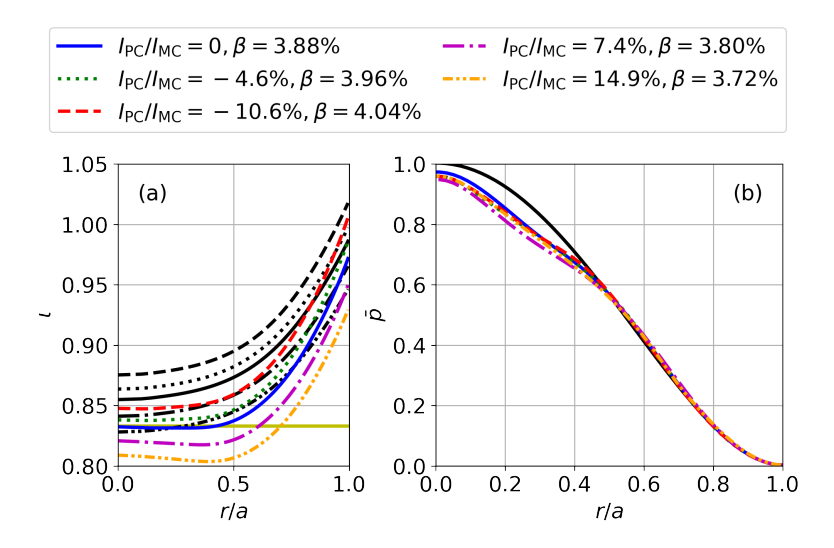


FIG. 4. (a) The rotational transform profiles in the simulated finite- β equilibria (colored), with the vacuum profiles (black) shown for comparison. The yellow line marks the $\iota=5/6$ resonance. (b) The final shapes of the pressure profile in the M3D- C^1 simulations, with the initial shape (solid) shown for comparison.

For finite- β equilibria, we use the peaked profile in Sec. 4 and adjust β so that the linear growth rates are comparable ($\gamma \approx 0.07~\mu s^{-1}$). The corresponding finite- β rotational transform profiles are shown by the colored curves in Fig. 4(a). Notably, an $\iota = 5/6$ resonance is present for positive I_{PC} and absent for negative I_{PC} . In Fig. 4(b), we present the saturated pressure profiles in full-torus simulations, which show similar levels of degradation despite the varying rotational transform and the presence or absence of the $\iota = 5/6$ resonance. This result implies that the core activities that lead to profile degradation might be of non-resonant nature [18]. It also suggests the possibility of developing a reduced theory to predict the saturation amplitude or state.

6. SUMMARY AND DISCUSSION

In this paper, we present comprehensive MHD simulations of ideal ballooning modes in high- β W7-X plasmas, building on our recent work that predicts benign saturation [8]. First, we find that while increasing the parallel thermal conductivity reduces the linear growth rate, the impact on the saturated pressure profile is limited. Second, we show that an equilibrium with a peaked profile and lower β is subject to more significant degradation than a broad profile and higher β , suggesting that benign saturation, or nonlinear stability, is by no means guaranteed. Third, we vary the equilibrium rotational transform by adjusting the planar coil current, and find that similar growth rates result in similar magnitudes of profile change regardless of the presence of a low-order resonance, which implies that the core activities that lead to the degradation may be of non-resonant nature. These results indicate that MHD stability should still be treated seriously in stellarator operation and design, for which nonlinear modelling using tools like M3D- C^1 can play an instrumental role.

That said, a full-torus M3D- C^1 simulation typically takes tens of thousands of CPU hours, which is too costly for iterative optimization of operation scenarios or device designs. To incorporate nonlinear stability considerations in these applications, a reduced model for predicting the nonlinear saturation amplitude or state needs to be formulated. Simulation results such as those in Sec. 4 imply such a possibility and can offer useful insights and help verify the reduced model.

ACKNOWLEDGEMENTS

Y.Z. is supported by the National MCF R&D Program under Grant Number 2024YFE03230400, the National Natural Science Foundation of China under Grant Number 12305246, and the Fundamental Research Funds for the Central Universities. N.M.F. is supported by the U.S. Department of Energy under contract number DE-AC02-09CH11466. The United States Government retains a non-exclusive, paid-up, irrevocable, world-wide license to publish or reproduce the published form of this manuscript, or allow others to do so, for United States Government purposes.

REFERENCES

- [1] Allen H. Boozer. "Physics of magnetically confined plasmas". In: *Rev. Mod. Phys.* 76.4 (Jan. 2005), pp. 1071-1141. ISSN: 0034-6861. DOI: 10.1103/RevModPhys.76.1071. URL: http://link.aps.org/doi/10.1103/RevModPhys.76.1071.
- [2] C. D. Beidler et al. "Demonstration of reduced neoclassical energy transport in Wendelstein 7-X". In: *Nature* 596.7871 (Aug. 2021), pp. 221–226. ISSN: 0028-0836. DOI: 10.1038/s41586-021-03687-w. URL: https://www.nature.com/articles/s41586-021-03687-w.
- [3] O. Grulke et al. "Overview of the first Wendelstein 7-X long pulse campaign with fully water-cooled plasma facing components". In: *Nucl. Fusion* 64.11 (Nov. 2024), p. 112002. ISSN: 0029-5515. DOI: 10.1088/1741-4326/ad2f4d. URL: https://iopscience.iop.org/article/10.1088/1741-4326/ad2f4d.
- [4] A. Langenberg et al. "Achieving stationary high performance plasmas at Wendelstein 7-X". In: *Phys. Plasmas* 31.5 (2024). ISSN: 10897674. DOI: 10.1063/5.0199958.
- [5] Craig Beidler et al. "Physics and engineering design for Wendelstein VII-X". In: Fusion Technol. 17.1 (1990), pp. 148–168. ISSN: 07481896. DOI: 10.13182/FST90-A29178.
- [6] G Grieger et al. "Physics optimization of stellarators". In: Phys. Fluids B Plasma Phys. 4.7 (Mar. 1992), pp. 2081–2091. ISSN: 0899-8221. DOI: 10.1063/1.860481. URL: http://aip.scitation. org/doi/10.1063/1.860481.
- [7] A. Weller et al. "Significance of MHD Effects in Stellarator Confinement". In: Fusion Sci. Technol. 50.2 (Aug. 2006), pp. 158-170. ISSN: 1536-1055. DOI: 10.13182/FST06-A1231. URL: https://www.tandfonline.com/doi/full/10.13182/FST06-A1231.
- [8] Yao Zhou et al. "Benign Saturation of Ideal Ballooning Instability in a High-Performance Stellarator". In: *Phys. Rev. Lett.* 133.13 (Sept. 2024), p. 135102. ISSN: 0031-9007. DOI: 10.1103/PhysRevLett. 133.135102. URL: https://link.aps.org/doi/10.1103/PhysRevLett.133.135102.
- [9] Yao Zhou et al. "Approach to nonlinear magnetohydrodynamic simulations in stellarator geometry". In: *Nucl. Fusion* 61.8 (Aug. 2021), p. 086015. ISSN: 0029-5515. DOI: 10.1088/1741-4326/ac0b35. URL: https://iopscience.iop.org/article/10.1088/1741-4326/ac0b35.

- [10] S. C. Jardin et al. "Multiple timescale calculations of sawteeth and other global macroscopic dynamics of tokamak plasmas". In: *Comput. Sci. Discov.* 5.1 (May 2012), p. 014002. ISSN: 1749-4699. DOI: 10. 1088/1749-4699/5/1/014002. URL: http://stacks.iop.org/1749-4699/5/i=1/a=014002?key=crossref.8be6a85f5fe84949a5c6782cbdf6adf5.
- [11] S.C. Jardin. "Review of implicit methods for the magnetohydrodynamic description of magnetically confined plasmas". In: *J. Comput. Phys.* 231.3 (Feb. 2012), pp. 822–838. ISSN: 00219991. DOI: 10.1016/j.jcp.2010.12.025. URL: http://dx.doi.org/10.1016/j.jcp.2010.12.025.
- [12] Yao Zhou, K Aleynikova, and N M Ferraro. "Nonlinear magnetohydrodynamic modeling of current-drive-induced sawtooth-like crashes in the W7-X stellarator". In: *Phys. Plasmas* 30.3 (Mar. 2023), p. 032503. ISSN: 1070-664X. DOI: 10.1063/5.0136654. URL: https://doi.org/10.1063/5.0136654. 0136654%20https://aip.scitation.org/doi/10.1063/5.0136654.
- [13] S P Hirshman. "Steepest-descent moment method for three-dimensional magnetohydrodynamic equilibria". In: *Phys. Fluids* 26.12 (1983), p. 3553. ISSN: 00319171. DOI: 10.1063/1.864116. URL: https://aip.scitation.org/doi/10.1063/1.864116.
- [14] M. Hölzl et al. "Determination of the heat diffusion anisotropy by comparing measured and simulated electron temperature profiles across magnetic islands". In: 49.11 (2009), p. 115009. DOI: 10.1088/0029-5515/49/11/115009. URL: https://dx.doi.org/10.1088/0029-5515/49/11/115009.
- [15] S.C. Jardin. "A triangular finite element with first-derivative continuity applied to fusion MHD applications". In: *J. Comput. Phys.* 200.1 (Oct. 2004), pp. 133-152. ISSN: 00219991. DOI: 10.1016/j.jcp.2004.04.004. URL: https://linkinghub.elsevier.com/retrieve/pii/S0021999104001366.
- [16] R. Sanchez et al. "COBRA: An Optimized Code for Fast Analysis of Ideal Ballooning Stability of Three-Dimensional Magnetic Equilibria". In: *J. Comput. Phys.* 161.2 (July 2000), pp. 576–588. ISSN: 00219991. DOI: 10.1006/jcph.2000.6514. URL: https://linkinghub.elsevier.com/retrieve/pii/S0021999100965148.
- [17] J. Geiger et al. "Physics in the magnetic configuration space of W7-X". In: *Plasma Phys. Control. Fusion* 57.1 (Jan. 2015), p. 014004. ISSN: 0741-3335. DOI: 10.1088/0741-3335/57/1/014004. URL: https://iopscience.iop.org/article/10.1088/0741-3335/57/1/014004.
- [18] A. M. Wright et al. "Predicting nonresonant pressure-driven MHD modes in equilibria with low magnetic shear". In: *Phys. Plasmas* 28.1 (Jan. 2021). ISSN: 1070-664X. DOI: 10.1063/5.0032489. URL: https://doi.org/10.1063/5.0032489%20https://pubs.aip.org/pop/article/28/1/012106/1031996/Predicting-nonresonant-pressure-driven-MHD-modes.